Article

ACCOUNTS
of chemical research

# Design, Synthesis, Assembly, and Engineering of Peptoid Nanosheets

Ellen J. Robertson, Alessia Battigelli, Caroline Proulx, Ranjan V. Mannige, Thomas K. Haxton, Lisa Yun, Stephen Whitelam, and Ronald N. Zuckermann*

Molecular Foundry, Lawrence Berkeley National Laboratory, Berkeley, California 94720, United States

CONSPECTUS: Two-dimensional (2D) atomically defined organic nanomaterials are an important material class with broad applications. However, few general synthetic methods exist to produce such materials in high yields and to precisely functionalize them. One strategy to form ordered 2D organic nanomaterials is through the supramolecular assembly of sequence-defined synthetic polymers. Peptoids, one such class of polymer, are designable bioinspired heteropolymers whose main-chain length and monomer sequence can be precisely controlled. We have recently discovered that individual peptoid polymers with a simple sequence of alternating hydrophobic and ionic monomers can self-assemble into highly ordered, free-floating nanosheets. A detailed understanding of their molecular structure and supramolecular assembly dynamics provides a robust platform for the discovery of new classes of nanosheets with tunable properties and novel applications.

In this Account, we discuss the discovery, characterization, assembly, molecular modeling, and functionalization of peptoid nanosheets. The fundamental properties of peptoid nanosheets, their mechanism of formation, and their application as robust scaffolds for molecular recognition and as templates for the growth of inorganic minerals have been probed by an arsenal of experimental characterization techniques (e.g., scanning probe, electron, and optical microscopy, X-ray diffraction, surface-selective vibrational spectroscopy, and surface tensiometry) and computational techniques (coarse-grained and atomistic modeling). Peptoid nanosheets are supramolecular assemblies of 16—42-mer chains that form molecular bilayers. They span tens of microns in lateral dimensions and freely float in water. Their component chains are highly ordered, with chains nearly fully extended and packed parallel to one another as a result of hydrophobic and electrostatic interactions. Nanosheets form via a novel interface-catalyzed monolayer collapse mechanism. Peptoid chains first assemble into a monolayer at either an air—water or oil—water interface, on which peptoid chains extend, order, and pack into a brick-like pattern. Upon mechanical compression of the interface, the monolayer buckles into stable bilayer structures.

Recent work has focused on the design of nanosheets with tunable properties and functionality. They are readily engineerable, as functional monomers can be readily incorporated onto the nanosheet surface or into the interior. For example, functional hydrophilic "loops" have been displayed on the surfaces of nanosheets. These loops can interact with specific protein targets, serving as a potentially general platform for molecular recognition. Nanosheets can also bind metal ions and serve as 2D templates for mineral growth. Through our understanding of the formation mechanism, along with predicted features ascertained from molecular modeling, we aim to further design and synthesize nanosheets as robust protein mimetics with the potential for unprecedented functionality and stability.
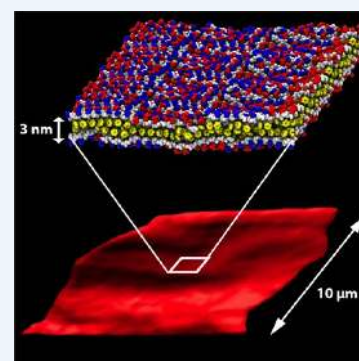
■ INTRODUCTION

Peptoids are peptidomimetic polymers composed of repeating N-substituted glycine monomer units, where the side chain is appended to the nitrogen atom rather than the α-carbon.[1] This subtle structural modification enhances their resistance to proteolysis,[2] rivaling the robustness of synthetic polymers, yet allows a high degree of chemically diverse sequence information to be encoded into the chain (Figure 1a).

The lack of both backbone chirality and backbone hydrogen-bond donors in peptoids results in a unique system where the propensity to adopt secondary structures and undergo supramolecular self-assembly is predominantly governed by side-chain—side-chain interactions. The solid-phase submonomer peptoid synthesis procedure[3,4] uses readily available bromoacetic acid and amine submonomers to install N-

substituted glycines one monomer at a time, allowing complete control over (1) the chain length, (2) the side-chain chemistry, and (3) the monomer sequence (Figure 1b). Hundreds of amine submonomers can be incorporated in excellent yields, giving access to a wide array of side chains. Peptoids are typically synthesized on a 100 mg scale, with lengths up to 50 residues in good crude purities.[5] Purities of >95% can be achieved through preparative reversed-phase high-performance liquid chromatography. The solid-phase submonomer method provides a practical route to sequence-defined peptoid chains that can be used to mimic the architecture of folded proteins. Because hydrophobic collapse is one of the major driving forces
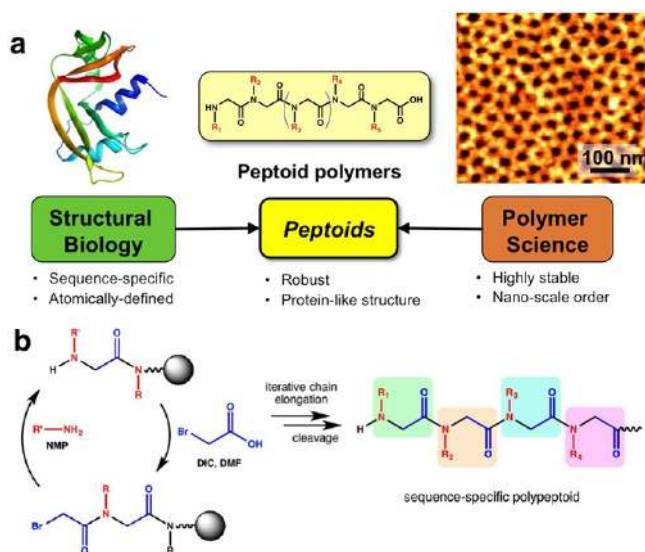
Figure 1. Peptoids are sequence-defined synthetic polymers. (a) Peptoids bridge a materials gap between the intricate, folded architectures found in proteins and the robustness and chemical diversity found in synthetic polymers. (b) Peptoids are efficiently synthesized via the solid-phase submonomer method to produce sequence-specific polymers of defined length.

in protein folding,[6] the design and synthesis of peptoids incorporating both hydrophobic (H) and polar (P) N-substituted glycine monomers in precise sequence arrangements has been explored in depth in recent years.[1] Specifically, en route toward mimicking protein structure and function, peptoids have demonstrated the ability to form a multitude of structures, including ribbons,[7] cyclic structures,[8−13] helices,[14,15] multihelical bundles,[16,17] superhelices,[18] and two-dimensional (2D) nanosheets.[19−24] Peptoid nanosheets are one of the most sophisticated protein-mimetic materials studied to date. Thus, this Account will focus on the synthesis, characterization, functionalization, and computational modeling of peptoid nanosheets.

■ PEPTOID NANOSHEET DISCOVERY AND CHARACTERIZATION

It is well-established that hydrophobic−hydrophilic sequence patterning plays a pivotal role in protein folding.[25] Additionally, aromatic and electrostatic interactions play key roles in supramolecular self-assembly.[25] With this knowledge, we designed a library of amphiphilic peptoids that explored different sequence patterns made from a minimal monomer set consisting of one hydrophobic monomer, N-(2-phenylethyl)glycine (Npe), and a pair of ionic monomers, N-(2-aminoethyl)glycine (Nae) and N-(2-carboxyethyl)glycine (Nce).[19] Pairs of complementary peptoids with a fixed length of 36 residues were synthesized and purified, alternating between aromatic and ionic monomers with twofold [(Nae-Npe)$_{18}$ (**1**) and (Nce-Npe)$_{18}$ (**2**); Figure 2a], threefold [(Nae-Npe-Npe)$_{12}$ and (Nce-Npe-Npe)$_{12}$], and fourfold [(Nae-Npe-Npe-Npe)$_9$ and (Nce-Npe-Npe-Npe)$_9$] periodicities. When these were mixed in equimolar ratios in aqueous buffer under physiological conditions, only the equimolar mixture of **1** and **2** was capable of assembling into free-floating nanosheets in high yield (Figure 2b). In order to make a single chain with all the necessary assembly information encoded into a single sequence, as in a protein, we extended the twofold periodic patterning design to
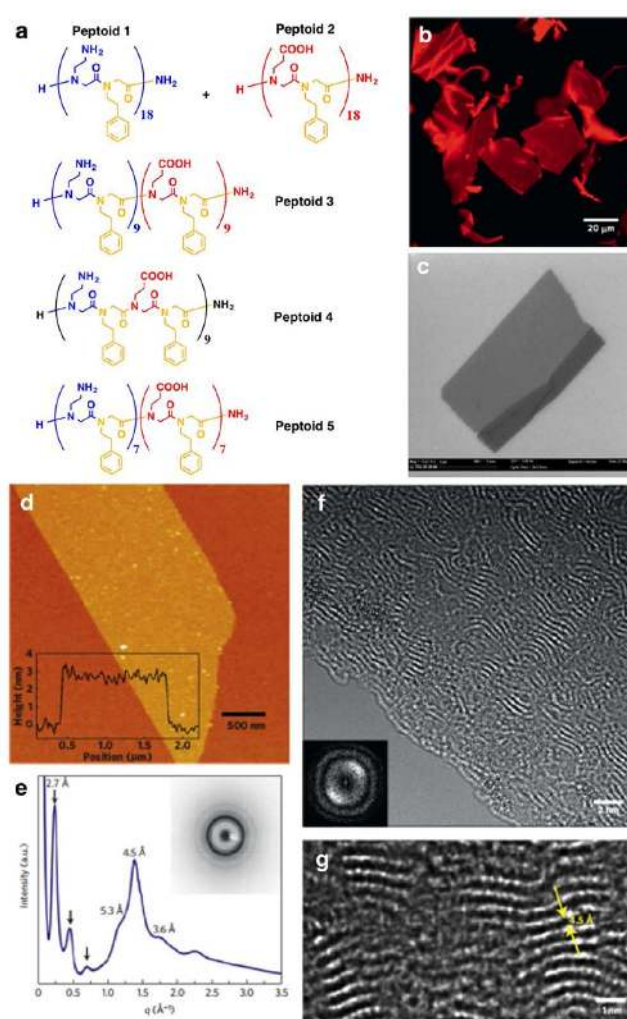

Figure 2. Characterization of nanosheets formed from peptoids with twofold aromatic−ionic periodicity. (a) Chemical structures of peptoids that were found to form nanosheets. (b) Fluorescence microscopy images of free-floating nanosheets stained with Nile Red. (c) SEM image of a nanosheet deposited on a plasma-etched silicon substrate. (d) AFM image of a nanosheet deposited on mica in ambient air. (e) XRD spectrum of dry stacked nanosheets. (f, g) Aberration-corrected TEM image of a nanosheet showing an interchain spacing of 4.5 Å. Adapted with permission from ref 19. Copyright 2010 Macmillan Publishers Limited.

produce peptoids with either block-charge domains [(Nae-Npe)$_9$−(Nce-Npe)$_9$ (**3**); Figure 2a] or alternating-charge monomers [(Nae-Npe-Nce-Npe)$_9$ (**4**); Figure 2a]. Both sequences formed nanosheets, but those obtained from **3** were more stable than those obtained from **4**, as revealed by resistance to changes in pH and organic solvent composition. Electrostatic calculations indicated that within the nanosheets, block-charge peptoids make more favorable interpeptoid electrostatic interactions than do alternating-charge peptoids.[20] Thus, nanosheets made from block-charge, single-chain peptoids are more stable than those made from alternating-charge ones. This greater stability is in part due to the energetic penalty associated with translating a peptoid chain relative to its neighboring strands within the nanosheet, which results in an increase in unfavorable intermolecular electrostatic interactions. The current standard sheet-forming peptoid, **5** (Figure 2a), possesses this block design and contains only 28 residues.[22]
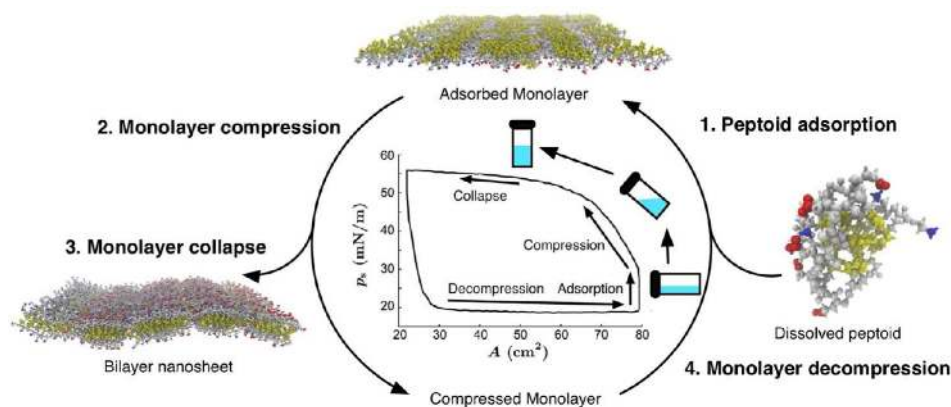
Figure 3. Nanosheet formation occurs through a key monolayer intermediate that forms at the air−water interface. Compression of this monolayer to form a bilayer is achieved by the vial-rocking method, as described by the surface pressure vs surface area isotherm for peptoid **5**. Adapted from ref 24. Copyright 2014 American Chemical Society.

This 28-residue peptoid is synthetically simpler to make than the longer ones, and forms nanosheets with structure and stability similar to those formed from the 36-residue peptoids.[22]

Peptoid nanosheets can be readily imaged in situ using both optical and fluorescence microscopy. For the latter, nanosheet-forming peptoids can be covalently labeled, or more simply, the nanosheet interior can be stained with Nile Red, an environmentally sensitive dye that fluoresces in hydrophobic environments. Unlabeled nanosheets can also be directly observed by differential interference contrast imaging. These techniques have shown that peptoid nanosheets have an extremely high aspect ratio with lengths and widths of hundreds of micrometers (area/thickness ratio >10^9 nm^{-1}) (Figure 2b).[19−24] These experimental observations pointed to a bilayer structure in which the hydrophobic groups are incorporated into the sheet interior and the hydrophilic groups are surface-exposed.

The nanosheets were further characterized using scanning electron microscopy (SEM), atomic force microscopy (AFM), X-ray diffraction (XRD), and aberration-corrected transmission electron microscopy (TEM).[19] SEM images (Figure 2c) showed that the nanosheets have very straight edges along one direction and conserve their structural integrity under high vacuum. AFM images of peptoid nanosheets in ambient air (Figure 2d) revealed a bilayer thickness of 2.7 nm with low surface roughness, indicating that the nanosheets are extremely flat and uniform across the sample. The XRD spectrum of dry pelleted nanosheets (Figure 2e) confirmed a sheet thickness of 2.7 nm and provided further information about the ordering at the molecular level, as revealed by the peaks at 5.3, 4.5, and 3.6 Å (vida infra). Aberration-corrected TEM analysis (Figure 2f) enabled direct visualization of peptoid strands and confirmed their extended backbone configuration. A close-up of the TEM image (Figure 2g) shows an interstrand spacing of 4.5 Å, consistent with the XRD results[19] and in close analogy to the distance of 4.7 Å found in peptide β-sheet secondary structures.[26]

Peptoid nanosheets are highly stable. Fluorescence recovery after photobleaching (FRAP) experiments showed that once the nanosheets are formed, there is no lateral mobility of peptoid chains within the nanosheets.[21] Nanosheets containing 1% fluorescently labeled peptoids were photobleached for 30 min and showed no fluorescence recovery after 1 h. In addition, the nanosheets persist in solution over long time periods. The assembly mechanism was probed by adding fluorescently labeled peptoids to a vial of nonfluorescent preformed nanosheets. Surprisingly, two distinct populations of sheets were observed, one fluorescent and one nonfluorescent. This indicates that once formed, nanosheets do not nucleate further growth. Because the nanosheets are held together by non-covalent aromatic and ionic interactions, variations in temperature, pH, organic solvent composition, and ionic strength can provide insights into nanosheet stability.[19,20] Interestingly, 1:1 mixtures of **1** and **2** were still able to produce nanosheets, albeit to a lesser extent, in the presence of up to 1 M NaCl. In addition, up to 50% acetonitrile in water was tolerated, as well wide ranges of temperature (up to 60 °C) and pH (pH 5−12). However, optimal nanosheet conditions were found to be in pH 8.0−9.0 Tris-HCl buffer (10 mM), where the two peptoid strands possess similar amounts of charge. This indicates that the hydrophobic interactions are likely the dominant driving force for assembly.

PEPTOID NANOSHEET FORMATION MECHANISM

Although nanosheet formation occurs with dilute (μM) aqueous solutions of peptoids, their formation does not occur through self-assembly in bulk solution.[21] Similar to Langmuir−Blodgett films,[27] nanosheet formation depends first on the ordered assembly of peptoids into a monolayer at either the air−water[21,22,24,28] or oil−water interface (Figure 3).[23] Subsequent collapse of this key monolayer intermediate produces bilayer peptoid nanosheets. On the basis of this unique mechanism, we developed a simple yet efficient and scalable method to produce nanosheets in high yields. Specifically, we built a custom vial-rocking device for nanosheet synthesis, where partially filled vials containing peptoid solutions are (1) held in a horizontal position for a set amount of time (typically a few minutes) to allow monolayer formation to occur, followed by (2) rotation to the vertical position, causing a decrease in the interfacial surface area that results in monolayer compression (Figure 3), and then back to the horizontal position.[21] This cycle can be repeated hundreds of times until >95% of the free peptoid has been depleted from the subphase and converted into nanosheets.[21]

Surface tension measurements were used to describe the events that occur during monolayer collapse and nanosheet formation.[21,24] Distinct regimes were observed in the surface pressure versus area isotherm (Figure 3): (1) adsorption and
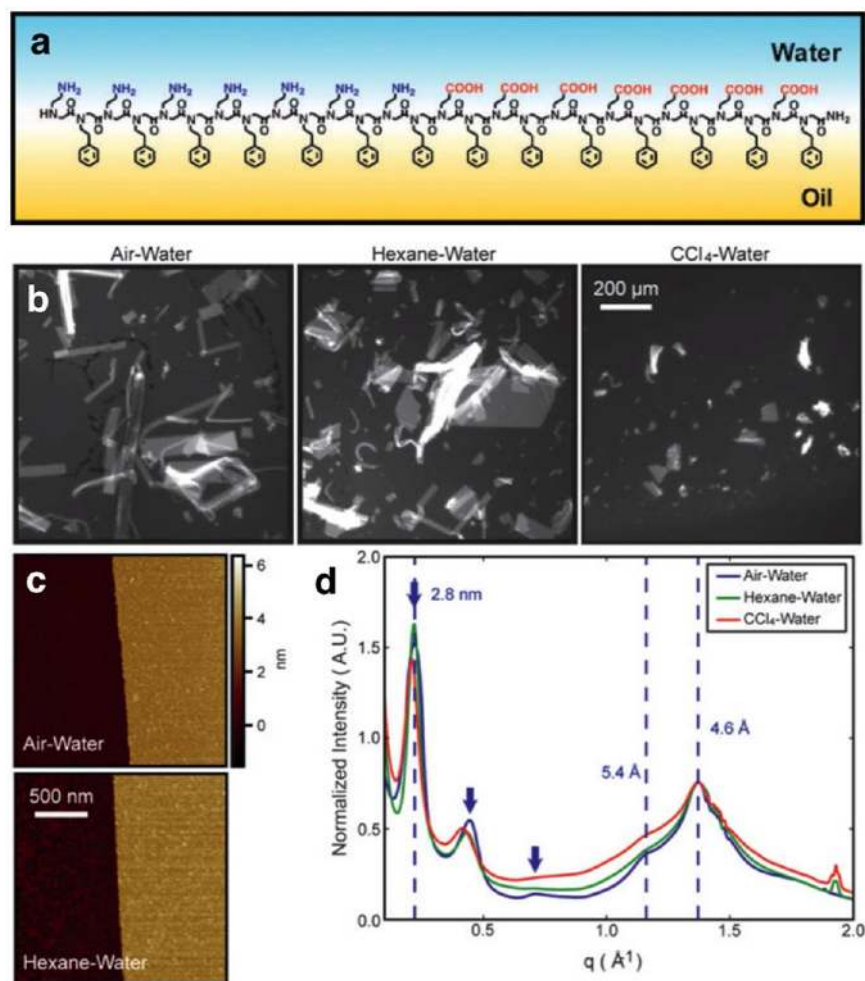
Figure 4. Nanosheet formation at the oil−water interface. (a) Cartoon depicting assembly of peptoid **5** at the oil−water interface. (b) Fluorescence microscopy images of nanosheets incubated with Nile Red that had assembled at different interfaces. (c) AFM images and (d) XRD spectra showing that nanosheets formed at different interfaces are structurally similar. Reproduced from ref 23.

ordering of **5** at the air−water interface to form a monolayer, (2) monolayer compression, (3) monolayer collapse into bilayers, (4) monolayer decompression, and then back to (1) peptoid readsorption. Both the appearance of a collapse point during compression and subsequent hysteresis during decompression revealed that bilayer formation is an irreversible process. Brewster angle microscopy showed that the monolayer experiences mechanical failure upon collapse,[21] indicating that buckling into the subphase relieves stress imparted by the compression. The collapse forces the hydrophobic *N*-2-phenylethyl groups into the bilayer interior to avoid interactions with the aqueous phase. The aromatic interactions between adjacent phenylethyl side chains promote the collapse event and contribute to subsequent nanosheet stability.

Peptoid nanosheet assembly can also occur at certain oil−water interfaces.[23] A series of hydrophobic fluids were tested for nanosheet formation with **5**, and it was found that not all hydrophobic solvents are effective (Figure 4b). Specifically, nanosheets were formed from short alkane solvents (e.g., hexane) but not from longer alkanes (e.g., hexadecane) or mineral oil, where high viscosity may interfere with monolayer collapse. Aromatic solvents (e.g., benzene, toluene) also inhibited sheet formation, likely because they interfere with π−π interactions between neighboring chains at the interface. Nanosheets were formed from the carbon tetrachloride−water

interface, which is an excellent solvent for vibrational spectroscopy (vida infra). These nanosheets were overall smaller and fewer than those made at the air−water and alkane−water interfaces because favorable interactions between the aromatic groups and CCl_4[29] may make monolayer detachment from the interface difficult. Characterization by AFM (Figure 4c) and XRD (Figure 4d) showed that nanosheets made from the oil−water interface are structurally similar to those formed from the air−water interface.[23]

Both the air−water and oil−water interfaces are confined locations where individual peptoid chains can concentrate and orient with one another. Because these interfaces can be continually regenerated for further peptoid adsorption and assembly, they serve as catalysts for nanosheet formation. The oil−water interface may additionally provide opportunities to produce nanosheets on microfluidic devices or to study coassembly with oil-soluble cargos. Such cargos have the potential to increase nanosheet stability and functionality.

■ ROLE OF MONOLAYER ORDERING

The formation of a stable and ordered peptoid monolayer is a pivotal step in the production of peptoid nanosheets. Therefore, a thorough understanding of the relationship between the monolayer and bilayer structures is essential to effectively use the interface as a platform for creating functional

nanosheets. X-ray scattering[24,28] and vibrational sum frequency (VSF)[23] spectroscopic studies of **5** were thus used to analyze the atomic-level structures and ordering in peptoid monolayers and bilayer nanosheets (Figure 5).[24,28]
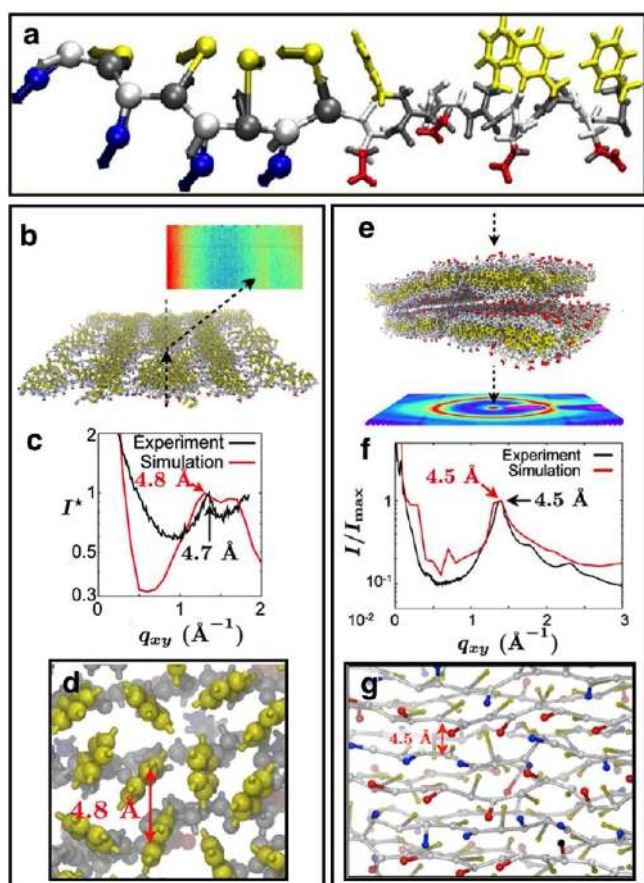

Figure 5. Comparison of calculated and experimental X-ray scattering results for the peptoid **5** monolayer and nanosheets. (a) Coarse-grained model of a block peptoid, in which monomers on the left are represented by coarse-grained sites and monomers on the right are back-mapped to the all-atom representation. (b, e) Scattering simulations of (b) the coarse-grained monolayer and (e) stacked nanosheets. (c, f) Experimental and simulated X-ray scattering spectra of (c) the monolayer and (f) stacked nanosheets. (d, g) Coarse-grained model of (d) the monolayer and (g) the bilayer showing similar lateral spacings between peptoid chains. Adapted from ref 24. Copyright 2014 American Chemical Society.

In order to provide a physical description of the monolayer and bilayer atomic-level structures as obtained through X-ray scattering experiments, we developed a coarse-grained model of associating peptoids (Figure 5a), which balances accuracy and efficiency. It represents backbone and side-chain sites using a minimal number of coarse-grained sites, making it much more efficient than all-atom models, but because sites possess independently fluctuating orientational degrees of freedom, the model can approach atomic-level accuracy.[24,28] Our coarse-grained model is capable of capturing processes on multiple time and length scales, ranging from fluctuations of individual side chains to the evolution of peptoid assemblies.

Scattering simulations of the coarse-grained monolayer model (Figure 5b) are able to replicate the experimental grazing-incidence X-ray spectrum of the monolayer (Figure 5c), revealing a characteristic in-plane distance near 4.8 Å. Both the

scattering simulations of the coarse-grained stacked nanosheet model (Figure 5e) and the corresponding experimental XRD studies produced spectra that displayed a similar distance near 4.5 Å (Figure 5f). The simulations revealed that these distances correspond to the spacing between parallel peptoid chains in the monolayer (Figure 5d) and nanosheet (Figure 5g), respectively. The simulations further described a second prominent feature in the monolayer spectrum that corresponds to a characteristic distance of ∼3.7 Å. We ascribe this distance to correlations between phenylethyl side chains, suggesting a liquidlike ordering of phenylethyl groups in the monolayer.

VSF spectroscopic measurements of **5** at the CCl_4-H_2O interface were used to probe peptoid monolayer ordering normal to the interfacial plane,[23] which was difficult to capture with X-ray scattering studies. Here, sharp peaks corresponding to the aromatic (~ 3066 cm^{-1}) and carboxylate (~ 1400 cm^{-1}) groups indicated a high degree of transverse ordering of these functional groups. This ordering is consistent with the aromatic ring ordering seen in the coarse-grained monolayer model.[24,28] Transverse ordering was also observed in the experimental and simulated "edge-on" XRD spectra of stacked bilayer nanosheets, both of which showed a peak at 5.6 Å corresponding to a combination of several contributions, including backbone–backbone and backbone–phenylethyl chain interactions.[24,28]

VSF spectroscopic measurements of **5** and its all-carboxylate analogue **6** were additionally performed to probe the role of intermolecular electrostatic interactions in monolayer ordering (Figure 6a).[23] A carboxylate peak near 1440 cm^{-1} appears in the spectrum of **5** that is absent in the spectrum of **6** and is ascribed to a direct electrostatic interaction between carboxylate and ammonium groups (Figure 6b). Repulsive interactions between the carboxylate groups prevent close packing and ordering in the monolayer of **6** (Figure 6c), inhibiting nanosheet formation under the same conditions as for **5**. These ionic interactions point to the importance of the relationship between peptoid sequence design and the ability to form a packed monolayer capable of collapse into nanosheets.

The combined X-ray scattering, VSF spectroscopic, and coarse-grained modeling studies illuminated that the ordering of peptoid chains within the nanosheets is achieved at the monolayer stage of assembly. Fine-tuning of the monolayer formation kinetics can therefore be employed to increase both the rate of nanosheet production and the nanosheet stability. Surface tension measurements as a function of temperature showed that peptoid adsorption to the air–water interface is the rate-limiting step in nanosheet formation.[24] Heating the peptoid solution increases the rate of peptoid adsorption and monolayer formation, resulting in a monolayer that is more saturated than unheated monolayers after the same amount of time. Annealing in the monolayer was also suggested, as sheets prepared under heating (60 °C) were observed to be more stable toward electron beam exposure than sheets prepared at room temperature.

◼ ATOMISTIC STRUCTURE OF PEPTOID NANOSHEETS

Engineering peptoid nanosheets for specific functionality requires a through understanding of the relationship between the peptoid monomer sequence and the resulting folded structure. Although the experimental results discussed above provide an in-depth picture of nanosheet formation and structure, resolving certain atomic-level details, such as the specific backbone conformation, requires atomistic molecular
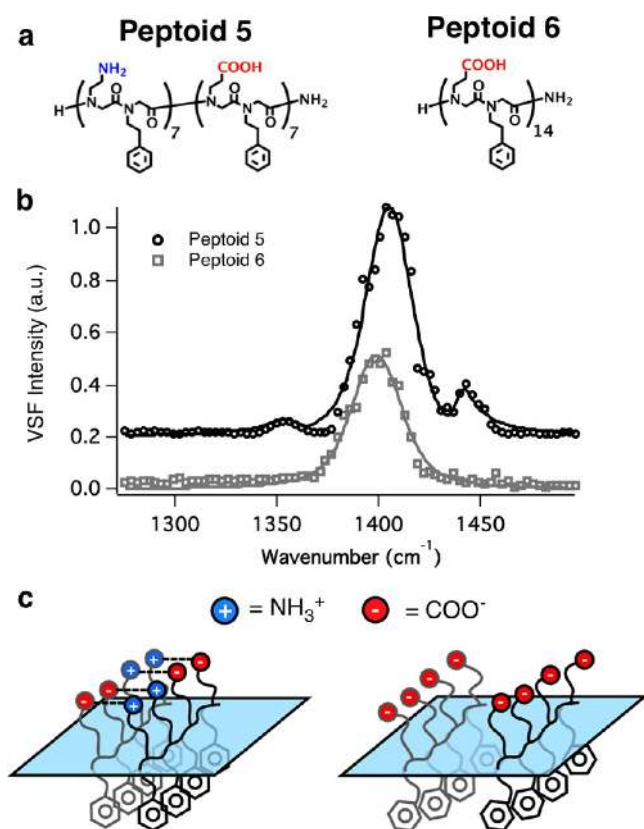
Figure 6. Attractive and repulsive electrostatic interactions in the monolayers of **5** and **6**, respectively. (a) Chemical structures of **5** and its all-carboxylate non-sheet-forming analogue **6**. (b) VSF spectra of the carboxylate-stretching region for peptoids **5** and **6** at the CCl_4–H_2O interface. (c) Cartoon representing attractive interactions in the **5** monolayer and repulsive interactions in the **6** monolayer. Adapted from ref 23.

Figure 7. Atomistic simulations of a peptoid nanosheet reveal a novel secondary structure. (a) Simulations show that nanosheets are flat because their backbones adopt a "Σ-strand" conformation (b), a secondary structure built from twist-opposed rotational states. (c) Backbones form a bricklike pattern that optimizes interactions between oppositely charged side chains, with pockets existing between chain termini. Adapted with permission from ref 31. Copyright 2015 Macmillan Publishers Limited.

modeling. We developed a CHARMM-based force field for peptoid polymers, MFTOID,[30] and used it to perform molecular dynamics (MD) simulations of a peptoid nanosheet[31] (Figure 7a).

Physical dimensions obtained from the simulations closely match those measured in the experiments, such as nanosheet thickness (28 vs 27 Å) and interpeptoid (4.8 vs 4.6 Å) and intra-side-chain (3.1 vs 3.6 Å) distances. The simulations also provided new understanding of the peptoid nanosheet structure at the atomic level. They showed that the macroscopic flatness of peptoid nanosheets is made possible because the peptoid backbones adopt a novel secondary structure, an alternating binary motif characterized by two regions on the Ramachandran plot (Figure 7b). We call this new secondary structure a "Σ-strand" because its characteristic twist-free nature is a consequence of the sum (or "Σ") of two rotational states.

The simulations of the peptoid nanosheet showed the existence of "pockets" (regions of few energetic interactions between peptoids) near the peptoid termini (Figure 7c). When pockets from the upper and lower bilayer leaflets align, water-porous channels are formed. The pockets are an integral part of a nanosheet's structure and may be useful for applications such as catalysis and selective membranes. The simulations also showed that nanosheets built from short polymers possess more pockets per unit area, and thus are less stable, than nanosheets built from long polymers. This prediction was confirmed by experiment: nanosheets composed of block-
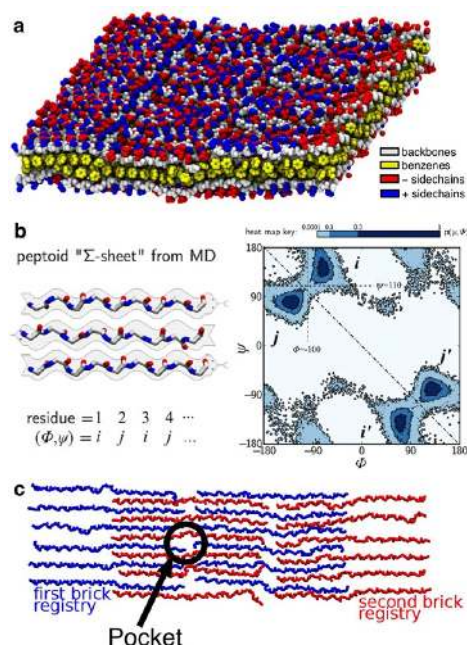
charge peptoids with lengths of 12 residues or shorter do not form stable nanosheets.

ENGINEERING FUNCTIONAL NANOSHEETS

The intriguing properties of peptoid nanosheets discussed above make this family of materials an extremely attractive scaffold for a wide range of functional applications such as biomolecular recognition, catalysis, and templating the growth of organic or inorganic structures. The ability to introduce a variety of chemically diverse monomers into the chain allows precise tuning of the peptoid structure and thus modulation of the properties of the resulting nanosheet assemblies. The chemical modification of the peptoid structure can be directed to the hydrophobic and/or hydrophilic domain, offering the opportunity to engineer the nanosheet interior and/or exterior, respectively. Engineering the hydrophobic domain can modulate the molecular packing interactions, thus impacting the stability, thickness, and porosity of the nanosheets, whereas engineering the hydrophilic domain can result in the multivalent surface display of complex functional groups. These modifications, together with the large surface area of the nanosheets, create a robust protein-mimetic platform for the specific binding of biological, chemical, or mineral species. Moreover, the surfaces of the nanosheets are zwitterionic, which can serve to reduce or eliminate the nonspecific adsorption of biomolecules.

The atomistic simulations of nanosheets predicted potentially useful properties to consider when designing peptoids for assembly into functional nanosheets. Specifically, the peptoid chains each possess different domains of structural rigidity (Figure 8a), with a greater flexibility observed at the peptoid termini and center.[31] These positions may be able to

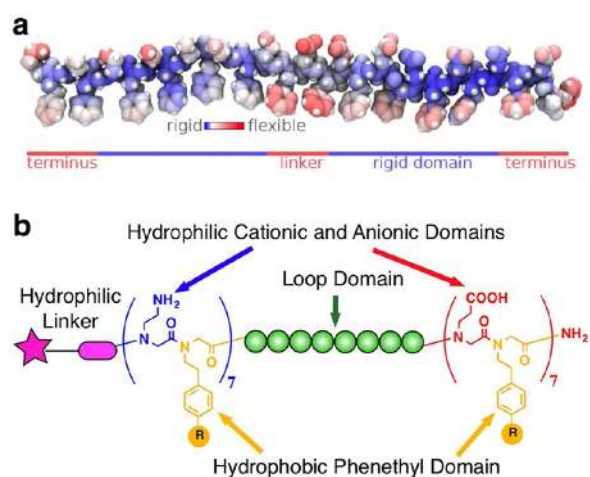accommodate the insertion of functional tags for molecular recognition.

Figure 8. Peptoid chain flexibility as related to rationalized functionalization. (a) Peptoid strand from an atomistic nanosheet simulation colored with respect to flexibility, showing three distinct regions of the backbone: a rigid domain, a flexible central linker, and flexible termini. (b) Peptoid design criteria for the functionalization of nanosheets. Panel (a) is reprinted with permission from ref 31. Copyright 2015 Macmillan Publishers Limited.

We have shown that it is possible to insert a specific tag on the N-terminus of the sheet-forming polymer using a hydrophilic linker (Figure 8b). Additionally, the insertion of different bioactive hydrophilic peptides in the middle of the amphiphilic peptoid sequence was designed to create surface-exposed loops, allowing subsequent interactions with target molecules.

As a proof of concept for the formation of biologically active nanosheets, a streptavidin-binding peptide sequence (cyclo-[CHPQFC]) was appended to the N-terminus of **1** to give functionalized peptoid **7** (Figure 9).[19] When **7** was mixed with **2**, nanosheets were obtained that were similar in abundance and morphology to nonfunctionalized nanosheets (Figure 9a). When a Cy3 fluorescently labeled streptavidin was used to evaluate protein binding to these nanosheets, high levels of fluorescence were observed, whereas a very weak signal was detected for the unfunctionalized nanosheets (Figure 9b,c). This demonstrated the possibility of effectively functionalizing the surface of peptoid nanosheets with a biologically active ligand without disrupting sheet formation.

The insertion of a peptide or peptoid domain in the middle of the sheet-forming peptoid strand can result in the creation of a high density of loops on the nanosheet surface, which can be tailored to display specific moieties. This strategy takes advantage of the mechanism of nanosheet formation, in which peptoids adsorb at the air–water interface with the hydrophobic moieties pointing into the air and hydrophilic moieties pointing into the water. Sufficiently hydrophilic loop domains are water-solvated upon peptoid adsorption, which are anchored to the surface by the flanking amphiphilic peptoid domains. During monolayer compression, the tight packing of aromatic groups in the hydrophobic domain results in exposure of the hydrophilic loops on the surface of the formed nanosheets (Figure 10a).
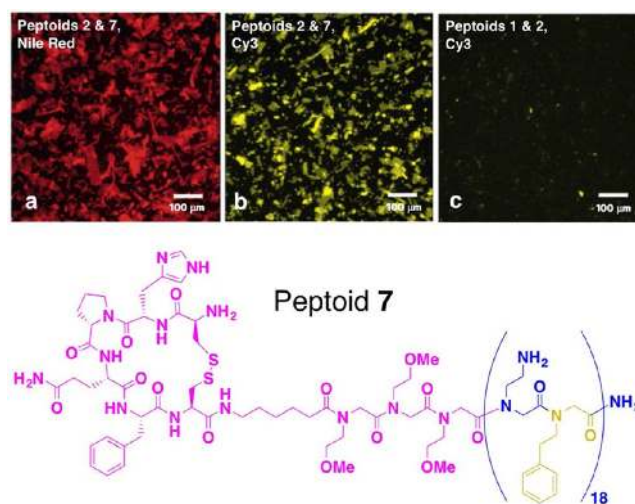

Figure 9. Binding of streptavidin to cyclic-peptide-functionalized peptoid nanosheets. (a) Nanosheets formed from mixing **7** (bottom) and **2**, visualized by fluorescence microscopy using Nile Red. (b, c) Functionalized and control nanosheets formed by (b) **7** and **2** and (c) **1** and **2** after incubation with Cy3-labeled streptavidin. The microscopy images are reprinted with permission from ref 19. Copyright 2010 Macmillan Publishers Limited.

The effective formation of loops on the nanosheet surface was studied with analogues of **5** in which homopolymers of N-(2-methoxyethyl)glycine (Nme) with different numbers of residues (0, 4, 8, or 12) were inserted in the middle of the peptoid sequence.[22] All of the analogues studied assembled into nanosheets, the structures of which were elucidated by AFM (Figure 10b–d) and XRD. AFM analysis highlighted that increasing the number of residues in the loop resulted in thicker sheets (~3–8 nm). This observation is consistent with the mechanism proposed, in which the hydrophilic loops are displayed on the surface of the nanosheets. Additionally, the larger loops resulted in greater surface roughness as determined by AFM, which was ascribed to enhanced surface disorder. Powder XRD analysis of the loop-containing nanosheets revealed a similar pattern observed in the unfunctionalized nanosheets with the characteristic peaks at 4.6 Å and 2.8 nm. The discrepancy in thickness as measured by AFM and XRD was attributed to the amorphous nature of the loop-containing nanosheet surface, which is too disordered to be detected by XRD.[22]

The formation mechanism of loop-exposed nanosheets was verified by comparing the monolayer thickness of the eight-residue-loop peptoid with that of **5** as a function of surface area, as measured by X-ray reflectivity.[22] Upon compression, the loop peptoid monolayer showed an increase in thickness that was not observed with a monolayer of **5**, consistent with the AFM results. As with **5**, a collapse point was observed in the surface pressure versus area isotherm of the loop peptoid monolayer. Together, these results indicate that the loops form during monolayer compression before collapse into nanosheets.

Further studies were performed on nanosheets with peptide loops. Specifically, **8** was synthesized with a peptide loop insert designed to bind gold atoms (vida infra). Because the submonomer method of peptoid synthesis is compatible with solid-phase peptide synthesis, the amino acids were readily incorporated into the loop domain.[22] Because the loop sequence was highly hydrophilic, the overall hydrophobicity of the sheet-forming segment was increased by replacing half of
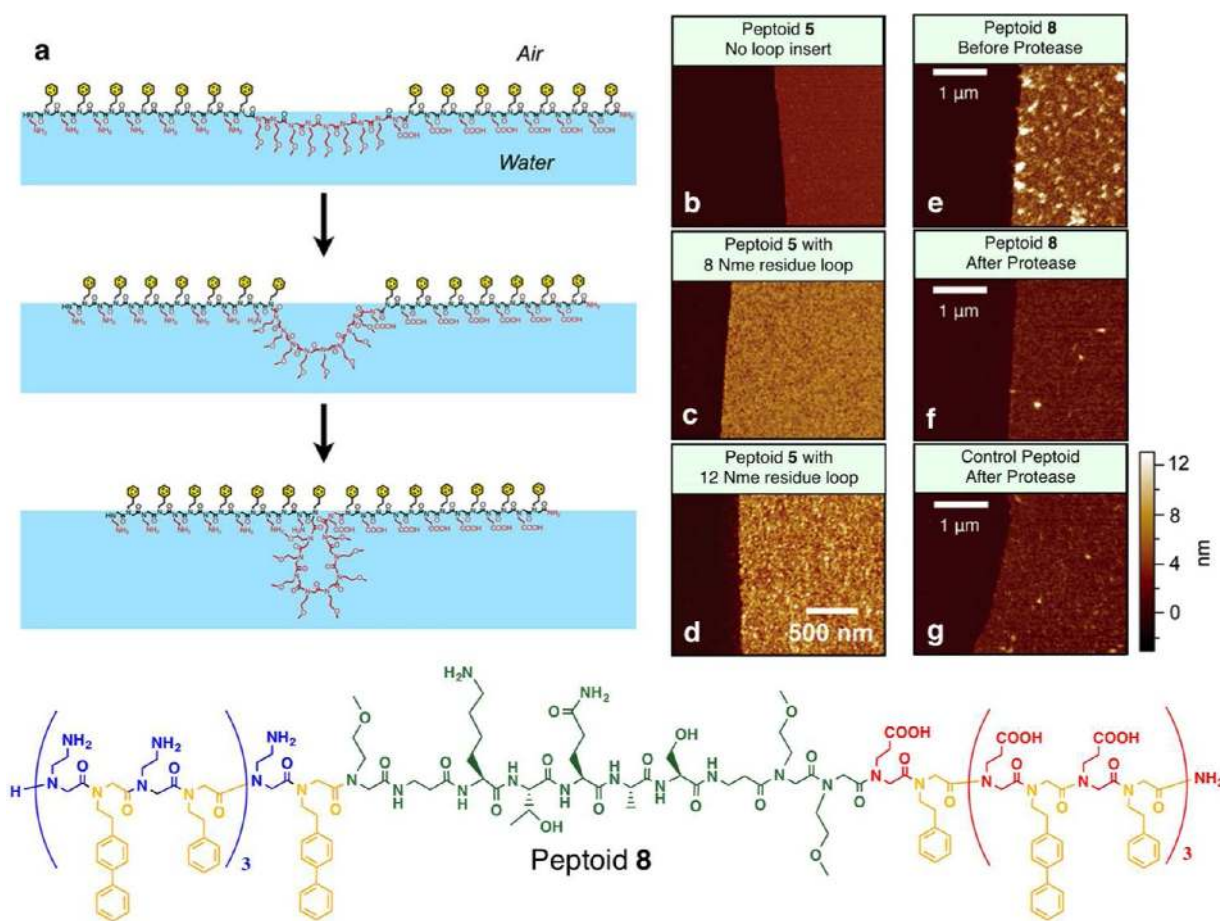
Figure 10. Peptoid nanosheets with functionalized loops. (a) Loop formation mechanism via monolayer compression. (b–d) AFM images of **5** with (b) no loop insert, (c) an 8 Nme residue loop, and (d) a 12 Nme residue loop. (e–g) AFM images of **8** (bottom) nanosheets (e) before and (f) after protease digestion compared with (g) control nanosheets. Adapted from ref 22. Copyright 2013 American Chemical Society.
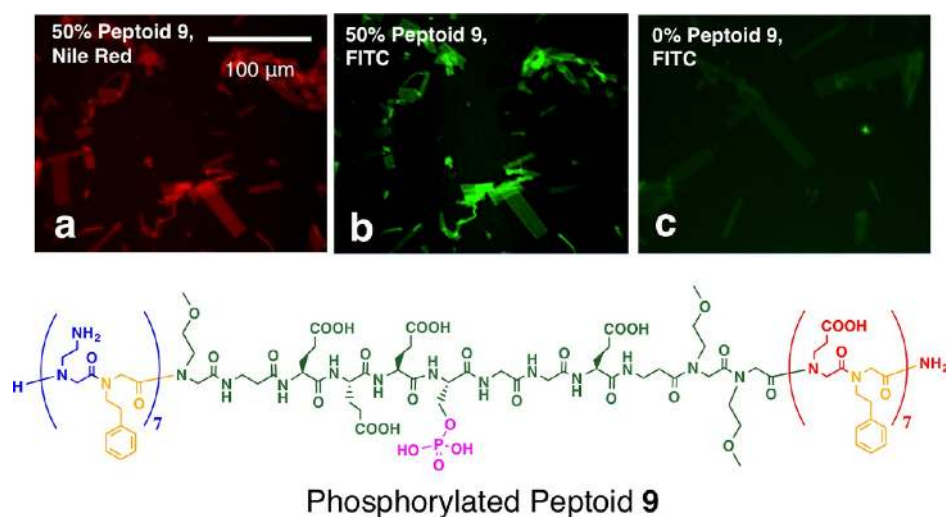

Figure 11. Antibody binding to loop-functionalized peptoid nanosheets. (a, b) Peptoids **5** and **9** (bottom) mixed at a ratio of 50% and (c) control peptoid **5**, each phosphorylated with CK2α followed by incubation with (a) Nile Red and (b, c) FITC-labeled anti-phosphoserine antibody. The microscopy images are reprinted from ref 22. Copyright 2013 American Chemical Society.

the aromatic residues with *N*-(2-(4-biphenyl)ethyl)glycine to allow adsorption at the air-water interface and the formation of stable peptoid nanosheets. To confirm that peptide loops were located only on the nanosheet exterior, nanosheets composed of **8** were incubated with a high concentration of Pronase, an

enzymatic cocktail of 10 different proteases.[22] Under optical microscopy no evident changes in nanosheet size, shape, and abundance were observed before and after the protease treatment. However, AFM analysis of the sheets (Figure 10e–g) revealed a significant reduction in the height and

roughness of the nanosheets after digestion, yielding measurements similar to those in nanosheets lacking the loop. This demonstrated that the peptide loops were indeed exposed on the surface and were accessible for recognition and cleavage by the proteases. Interestingly, the nanosheets remained intact despite the cleavage of each chain.

Our success in the ability to display peptoid and peptide loops on the surfaces of nanosheets led to the rational design of a loop sequence for the recognition of a specific protein target.[22] Insertion of the consensus nonapeptide sequence for casein kinase II (CK2α), anchored by three hydrophilic Nme residues to give **9** (Figure 11), was chosen because phosphorylation of the serine residue is readily detectable by immunofluorescence imaging or gel electrophoresis. Sheets with varying densities of surface-exposed loops were assembled by mixing different percentages of **9** (0, 0.5, 5 and 50%) with **5**. The nanosheets were incubated with CK2α and then with a fluorescently labeled monoclonal antibody specific for the phosphoserine residues. When the nanosheets contained a higher percentage of **9**, more fluorescence was observed, consistent with an increased number of phosphoserine residues. In contrast, the nanosheets without loops did not bind the fluorescent antibody (Figure 11a−c). The presence of phosphorylated peptide on the nanosheets was also detected by isoelectric focusing gel electrophoresis. The molecular recognition capability of loop-functionalized nanosheets demonstrated in this study has the potential to be used to detect a multitude of chemical and biological analytes depending upon the specific peptide/peptoid loop sequence. This should provide a family of robust molecular recognition elements that can be incorporated into a variety of sensing devices.

■ PEPTOID NANOSHEETS AS TEMPLATES FOR MINERAL GROWTH

Because of their large aspect ratio, stability, and defined structure, peptoid nanosheets are a promising platform to template the growth of inorganic structures. As such, a peptide sequence previously known to bind gold atoms was inserted in the center of **5** to give **8**.[22] Nanosheets with different loop densities were formed by mixing peptoid **8** and its unfunctionalized analogue in varying ratios and then incubated with a dilute solution of [AuCl$_4$]$^-$ ions. The resulting material was analyzed by AFM (Figure 12a,b). Sheets composed of 100% **8** displayed thick gold films on both sides of the nanosheets. Decreasing the percentage of **8** in the nanosheets resulted in more ordered and discrete nanostructures since their nucleation sites become further separated from one another.

We have also demonstrated that unfunctionalized nanosheets can serve as a platform for mineral growth. Because the zwitterionic nanosheet surface contains a high density of carboxylate groups, they are poised to bind metal ions though multivalent interactions. Thus, nanosheets formed of **5** were used as planar templates to promote the nucleation and growth of CaCO$_3$.[32] We have shown these nanosheets to be good scaffolds for the mineralization of thin amorphous CaCO$_3$ (ACC) films on their surface. Peptoid **5** nanosheets, supported on the surface of an agarose gel slice, were submerged in a CaCl$_2$ solution and subsequently exposed to CO$_2$ in a sealed chamber via ammonium carbonate diffusion. After 3 h of mineralization, the nanosheets were transferred to a silicon nitride substrate and analyzed by SEM, AFM, TEM, and
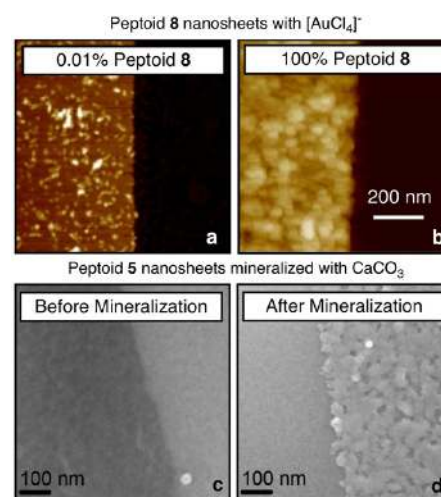

Figure 12. Mineralization of peptoid nanosheets. (a, b) AFM images of gold-decorated peptoid nanosheets formed from **8** and its unfunctionalized analogue at ratios of (a) 0.01% and (b) 100%. (c, d) SEM images of **5** nanosheets (c) before and (d) after CaCO$_3$ mineralization in solution. Panel (b) was reprinted from ref 22. Copyright 2013 American Chemical Society. Panels (c) and (d) were reprinted with permission from ref 32. Copyright 2015 Royal Society of Chemistry.

energy-dispersive X-ray spectroscopy (EDS). SEM images taken before and after mineralization showed an increase in the roughness of the mineralized material, with a continuous film characterized by a high density of partially coalesced spherical material consistent with the morphology of ACC (Figure 12c,d). The thickness of the mineralized nanosheets measured by AFM was 20 nm, with a mineralization growth rate of 2−3 nm h^{-1}. Analysis of the material by TEM and EDS revealed that the amorphous mineral could be converted into crystalline calcium oxide (a dehydration product of CaCO$_3$) under electron beam irradiation, further confirming the presence of ACC on the nanosheet surface. The ability to synthesize planar organic−inorganic composites holds great promise for the synthesis of nacre-mimetic materials, where the lamellar architecture can result in outstanding mechanical toughness.

■ CONCLUSIONS AND OUTLOOK

The formation of 2D organic nanomaterials with a defined molecular structure and protein-like function continues to be a challenge in materials science. Unlike most organic 2D nanomaterials reported in the literature,[33] peptoid nanosheets are a broad family of protein-like architectures that can be efficiently produced in high yields, can be readily functionalized at precise locations, and are biocompatible. Peptoid nanosheets have the potential to serve as atomically defined, robust nanoscale membranes, or scaffolds for a wide variety of applications, including molecular recognition and templated growth of layered materials. The well-developed combination of experimental and computational tools provide a unique platform to understand their molecular structure, the supramolecular mechanisms of assembly, and their resulting properties so that we may further increase the complexity and functionality of these 2D organic nanomaterials.

■ AUTHOR INFORMATION

Corresponding Author

*E-mail: rnzuckermann@lbl.gov.

Author Contributions

The manuscript was written through contributions of all authors. All authors have given approval to the final version of the manuscript.

Notes

The authors declare no competing financial interest.

Biographies

Ellen J. Robertson received her Ph.D. in chemistry in 2014 from the University of Oregon under the supervision of Prof. Geraldine L. Richmond. She then joined Ronald N. Zuckermann's group at Lawrence Berkeley National Laboratory as a Postdoctoral Fellow to study the physical properties of peptoid nanosheet formation.

Alessia Battigelli obtained her Ph.D. in 2012 in chemistry and pharmaceutical sciences from the University of Trieste and the University of Strasbourg under the co-supervision of Prof. Maurizio Prato and Dr. Alberto Bianco. In 2014 she joined Ronald N. Zuckermann's group at Lawrence Berkeley National Laboratory, where she is currently a postdoctoral fellow. Her research interests include the functionalization of nanomaterials and their biological applications.

Caroline Proulx received her Ph.D. in 2012 in organic chemistry from the Université de Montréal, working with Prof. William D. Lubell. She joined Ronald N. Zuckermann's laboratory at the Molecular Foundry as a Chemist Postdoctoral Fellow in 2012. Her research interests include the synthesis and study of conformationally constrained peptidomimetics.

Ranjan V. Mannige received his Ph.D. in computational biology from the Scripps Research Institute under the supervision of Charles L. Brooks, III. He then worked on biomolecular origination scenarios at Harvard University with Eugene Shakhnovich, after which he moved to his current postdoctoral position with Stephen Whitelam and Ronald Zuckerman at the Molecular Foundry, focusing on computational analysis of peptoid nanosheets. His research interests include protein origination, macromolecular design criteria, and systems biology.

Thomas K. Haxton received his Ph.D. in physics in 2010 from the University of Pennsylvania, where he was advised by Andrea Liu. He was a postdoctoral fellow at the Molecular Foundry from 2010 to 2015, advised by Stephen Whitelam and coadvised by Ronald Zuckermann starting in 2012. He is currently a Senior Data Scientist at Chegg.

Lisa Yun is an undergraduate research assistant in the Zuckermann lab, majoring in microbiology at UC Berkeley.

Stephen Whitelam is a scientist at the Molecular Foundry at Lawrence Berkeley National Laboratory. He studies nanoscale pattern formation and self-assembly. He received his Ph.D. in theoretical physics from Oxford University in 2004, where he worked with Juan P. Garrahan and David Sherrington. He did postdoctoral work from 2004 to 2007 with Phillip L. Geissler at UC Berkeley and from 2007 to 2008 with Nigel Burroughs at Warwick University.

Ronald N. Zuckermann is a Senior Scientist and Facility Director of the Biological Nanostructures Facility at the Molecular Foundry at the Lawrence Berkeley National Laboratory. He obtained a Ph.D. in chemistry from UC Berkeley in 1989 and worked as a research scientist in the biotechnology industry for 16 years developing combinatorial drug discovery technologies. He was named a Chiron Research Fellow in 2003 and an LBNL Senior Scientist in 2011. He invented sequence-defined peptoid polymers and works on folding them into precise nanoscale architectures. He adapts structural design rules from biology and applies them to the world of materials science.

■ REFERENCES

(1) Sun, J.; Zuckermann, R. N. Peptoid Polymers: A Highly Designable Bioinspired Material. *ACS Nano* **2013**, 7, 4715−4732.

(2) Miller, S. M.; Simon, R. J.; Ng, S.; Zuckermann, R. N.; Kerr, J. M.; Moos, W. H. Comparison of the Proteolytic Susceptibilities of Homologous L-Amino-Acid, D-Amino-Acid, and N-Substituted Glycine Peptide and Peptoid Oligomers. *Drug Dev. Res.* **1995**, 35, 20−32.

(3) Zuckermann, R. N.; Kerr, J. M.; Kent, S. B. H.; Moos, W. H. Efficient Method for the Preparation of Peptoids Oligo (N-Substituted Glycines) by Submonomer Solid-Phase Synthesis. *J. Am. Chem. Soc.* **1992**, 114, 10646−10647.

(4) Proulx, C.; Yoo, S.; Connolly, M. D.; Zuckermann, R. N. Accelerated Submonomer Solid-Phase Synthesis of Peptoids Incorporating Multiple Substituted N-Aryl Glycine Monomers. *J. Org. Chem.* **2015**, 80, 10490−10497.

(5) Murphy, J. E.; Uno, T.; Hamer, J. D.; Cohen, F. E.; Dwarki, V.; Zuckermann, R. N. A Combinatorial Approach to the Discovery of Efficient Cationic Peptoid Reagents for Gene Delivery. *Proc. Natl. Acad. Sci. U. S. A.* **1998**, 95, 1517−1522.

(6) Zarrine-Afsar, A.; Wallin, S.; Neculai, A. M.; Neudecker, P.; Howell, P. L.; Davidson, A. R.; Chan, H. S. Theoretical and Experimental Demonstration of the Importance of Specific Nonnative Interactions in Protein Folding. *Proc. Natl. Acad. Sci. U. S. A.* **2008**, 105, 9999−10004.

(7) Crapster, J. A.; Guzei, I. A.; Blackwell, H. E. A Peptoid Ribbon Secondary Structure. *Angew. Chem., Int. Ed.* **2013**, 52, 5079−5084.

(8) Shin, S. B. Y.; Yoo, B.; Todaro, L. J.; Kirshenbaum, K. Cyclic Peptoids. *J. Am. Chem. Soc.* **2007**, 129, 3218−3225.

(9) Shah, N. H.; Butterfoss, G. L.; Nguyen, K.; Yoo, B.; Bonneau, R.; Rabenstein, D. L.; Kirshenbaum, K. Oligo (N-Aryl Glycines): A New Twist on Structured Peptoids. *J. Am. Chem. Soc.* **2008**, 130, 16622−16632.

(10) Yoo, B.; Shin, S. B. Y.; Huang, M. L.; Kirshenbaum, K. Peptoid Macrocycles: Making the Rounds with Peptidomimetic Oligomers. *Chem. - Eur. J.* **2010**, 16, 5528−5537.

(11) Holub, J. M.; Jang, H.; Kirshenbaum, K. Fit to Be Tied: Conformation-Directed Macrocyclization of Peptoid Foldamers. *Org. Lett.* **2007**, 9, 3275−3278.

(12) Park, S.; Kwon, Y.-U. Facile Solid-Phase Parallel Synthesis of Linear and Cyclic Peptoids for Comparative Studies of Biological Activity. *ACS Comb. Sci.* **2015**, 17, 196−201.

(13) Lee, J. H.; Meyer, A. M.; Lim, H.-S. A Simple Strategy for the Construction of Combinatorial Cyclic Peptoid Libraries. *Chem. Commun. (Cambridge, U. K.)* **2010**, 46, 8615−8617.

(14) Wu, C. W.; Sanborn, T. J.; Huang, K.; Zuckermann, R. N.; Barron, A. E. Peptoid Oligomers with Alpha-Chiral, Aromatic Side Chains: Sequence Requirements for the Formation of Stable Peptoid Helices. *J. Am. Chem. Soc.* **2001**, 123, 6778−6784.

(15) Stringer, J. R.; Crapster, J. A.; Guzei, I. A.; Blackwell, H. E. Extraordinarily Robust Polyproline Type I Peptoid Helices Generated

Via the Incorporation of Alpha-Chiral Aromatic N-1-Naphthylethyl Side Chains. *J. Am. Chem. Soc.* **2011**, *133*, 15559−15567.

(16) Burkoth, T. S.; Beausoleil, E.; Kaur, S.; Tang, D. Z.; Cohen, F. E.; Zuckermann, R. N. Toward the Synthesis of Artificial Proteins: The Discovery of an Amphiphilic Helical Peptoid Assembly. *Chem. Biol.* **2002**, *9*, 647−654.

(17) Lee, B. C.; Zuckermann, R. N.; Dill, K. A. Folding a Nonbiological Polymer into a Compact Multihelical Structure. *J. Am. Chem. Soc.* **2005**, *127*, 10999−11009.

(18) Murnen, H. K.; Rosales, A. M.; Jaworski, J. N.; Segalman, R. A.; Zuckermann, R. N. Hierarchical Self-Assembly of a Biomimetic Diblock Copolypeptoid into Homochiral Superhelices. *J. Am. Chem. Soc.* **2010**, *132*, 16112−16119.

(19) Nam, K. T.; Shelby, S. A.; Choi, P. H.; Marciel, A. B.; Chen, R.; Tan, L.; Chu, T. K.; Mesch, R. A.; Lee, B.-C.; Connolly, M. D.; Kisielowski, C.; Zuckermann, R. N. Free-Floating Ultrathin Two-Dimensional Crystals from Sequence-Specific Peptoid Polymers. *Nat. Mater.* **2010**, *9*, 454−460.

(20) Kudirka, R.; Tran, H.; Sanii, B.; Nam, K. T.; Choi, P. H.; Venkateswaran, N.; Chen, R.; Whitelam, S.; Zuckermann, R. N. Folding of a Single-Chain, Information-Rich Polypeptoid Sequence into a Highly Ordered Nanosheet. *Biopolymers* **2011**, *96*, 586−595.

(21) Sanii, B.; Kudirka, R.; Cho, A.; Venkateswaran, N.; Olivier, G. K.; Olson, A. M.; Tran, H.; Harada, R. M.; Tan, L.; Zuckermann, R. N. Shaken, Not Stirred: Collapsing a Peptoid Monolayer to Produce Free-Floating, Stable Nanosheets. *J. Am. Chem. Soc.* **2011**, *133*, 20808−20815.

(22) Olivier, G. K.; Cho, A.; Sanii, B.; Connolly, M. D.; Tran, H.; Zuckermann, R. N. Antibody-Mimetic Peptoid Nanosheets for Molecular Recognition. *ACS Nano* **2013**, *7*, 9276−9286.

(23) Robertson, E. J.; Olivier, G. K.; Qian, M.; Proulx, C.; Zuckermann, R. N.; Richmond, G. L. Assembly and Molecular Order of Two-Dimensional Peptoid Nanosheets through the Oil-Water Interface. *Proc. Natl. Acad. Sci. U. S. A.* **2014**, *111*, 13284−13289.

(24) Sanii, B.; Haxton, T. K.; Olivier, G. K.; Cho, A.; Barton, B.; Proulx, C.; Whitelam, S.; Zuckermann, R. N. Structure-Determining Step in the Hierarchical Assembly of Peptoid Nanosheets. *ACS Nano* **2014**, *8*, 11674−11684.

(25) Berg, J. M.; Tymoczko, J. L.; Stryer, L. *Biochemistry*; W.H. Freeman: Basingstoke, U.K., 2012.

(26) Krejchi, M. T.; Atkins, E. D. T.; Waddon, A. J.; Fournier, M. J.; Mason, T. L.; Tirrell, D. A. Chemical Sequence Control of Beta-Sheet Assembly in Macromolecular Crystals of Periodic Polypeptides. *Science* **1994**, *265*, 1427−1432.

(27) Zasadzinski, J.; Viswanathan, R.; Madsen, L.; Garnaes, J.; Schwartz, D. Langmuir-Blodgett Films. *Science* **1994**, *263*, 1726−1733.

(28) Haxton, T. K.; Mannige, R. V.; Zuckermann, R. N.; Whitelam, S. Modeling Sequence-Specific Polymers Using Anisotropic Coarse-Grained Sites Allows Quantitative Comparison with Experiment. *J. Chem. Theory Comput.* **2015**, *11*, 303−315.

(29) Ahmed, A. Complex-Formation between Carbon-Tetrachloride and Alkyl-Substituted Benzenes. *J. Chem. Soc., Faraday Trans. 1* **1973**, *69*, 540−545.

(30) Mirijanian, D. T.; Mannige, R. V.; Zuckermann, R. N.; Whitelam, S. Development and Use of an Atomistic Charmm-Based Forcefield for Peptoid Simulation. *J. Comput. Chem.* **2014**, *35*, 360−370.

(31) Mannige, R. V.; Haxton, T. K.; Proulx, C.; Robertson, E. J.; Battigelli, A.; Butterfoss, G. L.; Zuckermann, R. N.; Whitelam, S. Peptoid Nanosheets Exhibit a New Secondary-Structure Motif. *Nature* **2015**, *526*, 415−420.

(32) Jun, J. M. V.; Altoe, M. V. P.; Aloni, S.; Zuckermann, R. N. Peptoid Nanosheets as Soluble, Two-Dimensional Templates for Calcium Carbonate Mineralization. *Chem. Commun. (Cambridge, U. K.)* **2015**, *51*, 10218−10221.

(33) Zhuang, X.; Mai, Y.; Wu, D.; Zhang, F.; Feng, X. Two-Dimensional Soft Nanomaterials: A Fascinating World of Materials. *Adv. Mater. (Weinheim, Ger.)* **2015**, *27*, 403−427.